Magnetic structure of mixed iron-gallium borate crystals

Kira Seleznyova, Mark Strugatsky, Sergey Yagupov, Yuliya Mogilenec, Patrick Rosa, Mathieu Gonidec, Janis Kliava

ARTICLE IN PRESS

Journal of Alloys and Compounds XXX (XXXX) XXXXXX

Contents lists available at ScienceDirect

Journal of Alloys and Compounds

journal homepage: www.elsevier.com/locate/jalcom

Magnetic structure of mixed iron-gallium borate crystals: EMR and SQUID studies

Kira Seleznyova [a], Mark Strugatsky [a], Sergey Yagupov [a], Yuliya Mogilenec [a], Patrick Rosa [b], Mathieu Gonidec [b], Janis Kliava [c,*]

[a] Physics and Technology Institute, V.I. Vernadsky Crimean Federal University, 4 Vernadsky Ave., Simferopol 295007, Crimea, Russia
[b] CNRS, Univ. Bordeaux, Bordeaux INP, ICMCB, UMR 5026, F-33600 Pessac, France
[c] LOMA, UMR 5798 Université de Bordeaux-CNRS, 33405 Talence Cedex, France

ARTICLE INFO

Keywords:
Iron-gallium borates
Superparamagnetism
Electron magnetic resonance
SQUID magnetometry

ABSTRACT

Iron-gallium borate, $Fe_xGa_{1-x}BO_3$, single crystals have been synthesized by the solution in the melt technique. The exact x-values in the crystals have been determined by X-ray fluorescence analysis and checked by Energy Dispersive X-Ray Spectroscopy. Scanning Electron Microscopy has been used to map distributions of iron and gallium ions in the crystals. The electron magnetic resonance (EMR) spectra as well as field and temperature dependences of the magnetization obtained by SQUID reveal the existence of different magnetic phases in different x ranges, *viz.* weakly ferromagnetic antiferromagnetic, magnetic cluster and paramagnetic phase. For crystals with $0.32 \leq x \leq 0.83$, the Néel temperatures, T_N, have been determined. The magnetometry of these crystals suggests the existence of another magnetic transition at a temperature well below T_N, tentatively ascribed to a Morin type transition. Detailed EMR and SQUID studies of the crystal with $x \approx 0.2$ reveal the existence of magnetic nanoclusters showing superparamagnetic behaviour. Using a laboratory developed code based on the Monte-Carlo technique, spatial distributions of dia- and paramagnetic ions in the crystal with $x \approx 0.2$ has been visualized and possible cluster sizes have been estimated.

1. Introduction

Iron borate, $FeBO_3$, – a trigonal antiferromagnet with weak ferromagnetism – exemplifies a class of materials that can be called "transparent magnets", as far as they combine a room-temperature magnetism and a transmission window in the visible spectral range [1]. Its amazing magnetic, magneto-acoustic, optical, magneto-optical, *etc.* properties [1–17] make it a promising candidate for applications in various branches of science and technology. In particular, instruments for measuring ultra-weak magnetic fields, temperature and pressure, magneto-optical and magneto-acoustic transducers as well as excellent monochromators for synchrotron Mössbauer spectroscopy can be made on its basis [18–21]. However, the performances of such applications depend on the possibility of fine-tuning magnetic characteristics of the basic material, *e.g.*, the Néel temperature T_N as well as the Dzyaloshinskii-Moriya, exchange and magnetocrystalline anisotropy fields. Such fine-tuning can be attained by diamagnetically diluting iron borate, *i.e.*, partially substituting iron with diamagnetic ions [22].

In the last decade, by developing a dedicated synthesis technique, we have manufactured a series of diamagnetically diluted $Fe_xGa_{1-x}BO_3$ single crystals with $0 \leqslant x \leqslant 1$. All these crystals belong to D^6_{3d} space symmetry group and possesses, in particular, three two-fold axes that lie in the basal plane perpendicular to three-fold axis C_3 and are isostructural with $FeBO_3$ [23,24]. By gradually reducing x in these crystals, we have monitored the transition from magnetically ordered state to paramagnetism of isolated Fe(III) ions. Our Electron Magnetic Resonance (EMR) studies of this crystal series have revealed that T_N, the Dzyaloshinskii–Moriya field and the isotropic energy gap substantially decrease with decreasing x [22]. Besides, we have identified a partially ordered magnetic state emerging in these crystals at intermediate x-values [22,25]. Indeed, Fe(III) and Ga(III) have very similar ionic radii, respectively 0.645 and 0.620 Å in sixfold coordination [26] occurring in iron borate. Therefore, their distribution in mixed $Fe_xGa_{1-x}BO_3$ crystals is mostly random, resulting in the appearance of regions with different local concentrations of paramagnetic ions and implying different types of magnetic ordering; in particular, magnetic

* Corresponding author.
E-mail address: janis.kliava@u-bordeaux.fr (J. Kliava).

Received 5 August 2023; Received in revised form 10 November 2023; Accepted 8 December 2023

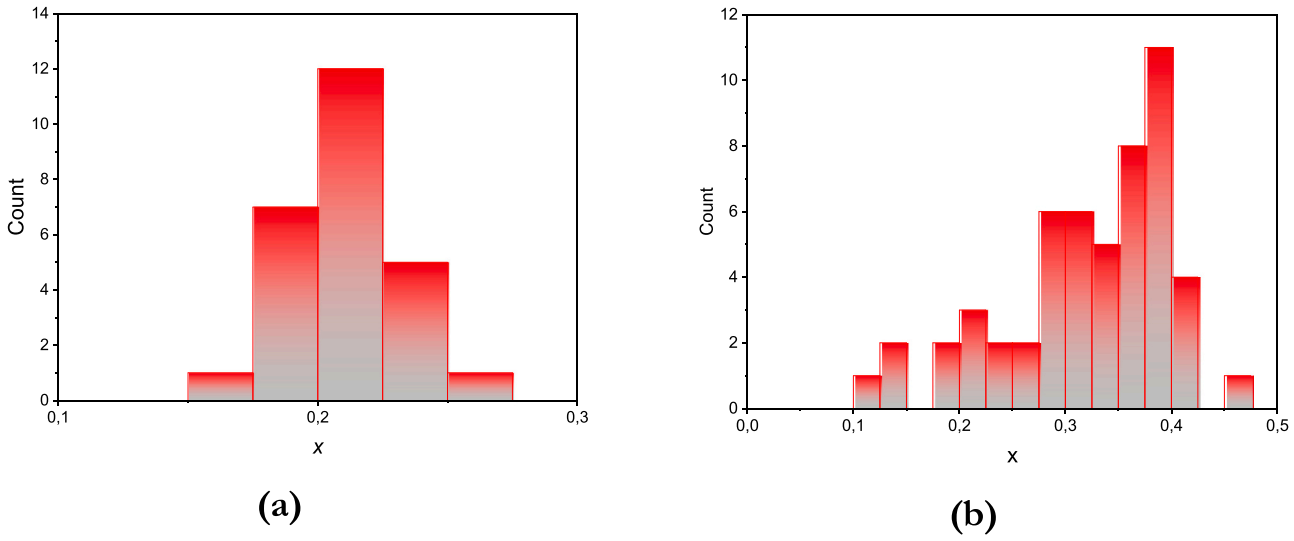

Fig. 1. Histograms of the distribution of x for crystals extracted from crucibles with $x_{charge} = 0.1$ (a) and 0.25 (b), obtained using EDS.

nanoclusters that under certain conditions can be considered as single-domain nanoparticles [27]. The anisotropy energy of such particles in a first approximation is proportional to their volume V [27]. For uniaxial anisotropy, the energy barrier separating the easy magnetization directions is $E_{barrier} = KV$, K being the corresponding constant [27]. For particles of a sufficiently small V, $E_{barrier}$ can be lower than the thermal excitation energy kT, k and T being the Boltzmann constant and the temperature, respectively. Thus, the energy barrier for a magnetization reversal is overcome and the orientation of the total magnetic moment of such particles fluctuates similarly to that of a single paramagnetic ion in a diluted paramagnet, although individual spins within the particles remain exchange-coupled until, T_N is reached. The type of magnetism of an assembly of such particles is referred to as *superparamagnetism*. Besides, the observed magnetic behaviour of the superparamagnetic particles depends on the ratio between the temporal window, or "measuring time", t_m of the experimental technique and the relaxation time τ associated with overcoming the energy barrier. It is usually considered that in the superparamagnetic regime the relation between τ and $E_{barrier}$ obeys the N é el–Arrhenius law:

$$\tau = \tau_0 \exp \frac{E_{barrier}}{kT}, \quad (1)$$

where the pre-exponential factor τ_0 can be considered as an average time between consecutive attempts to jump over the energy barrier. Typically, τ_0 lies in the range from 10^{-11} to 10^{-9} for ferromagnetic particles, from 10^{-13} to 10^{-12} for antiferromagnetic particles [27] and from 10^{-12} to 10^{-8} for molecular species or non-interacting single--domain superparamagnetic nanoparticles [28–30]. If the relaxation is fast, $\tau \ll t_m$, the average magnetization tends to zero. Such particles are in the superparamagnetic state, in which case their magnetic moments can

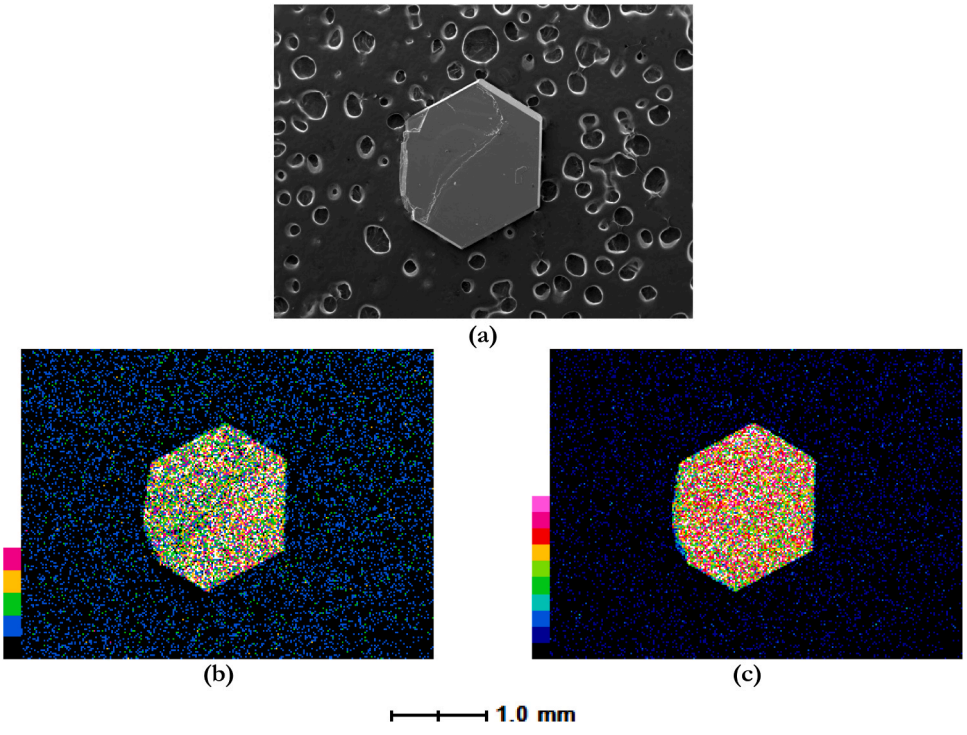

Fig. 2. SEM image (a) and mapping of Fe (b) and Ga (c) distributions in $Fe_xGa_{1-x}BO_3$ single crystal with $x = 0.2$. The (a) to (c) figures are shown on the same scale.

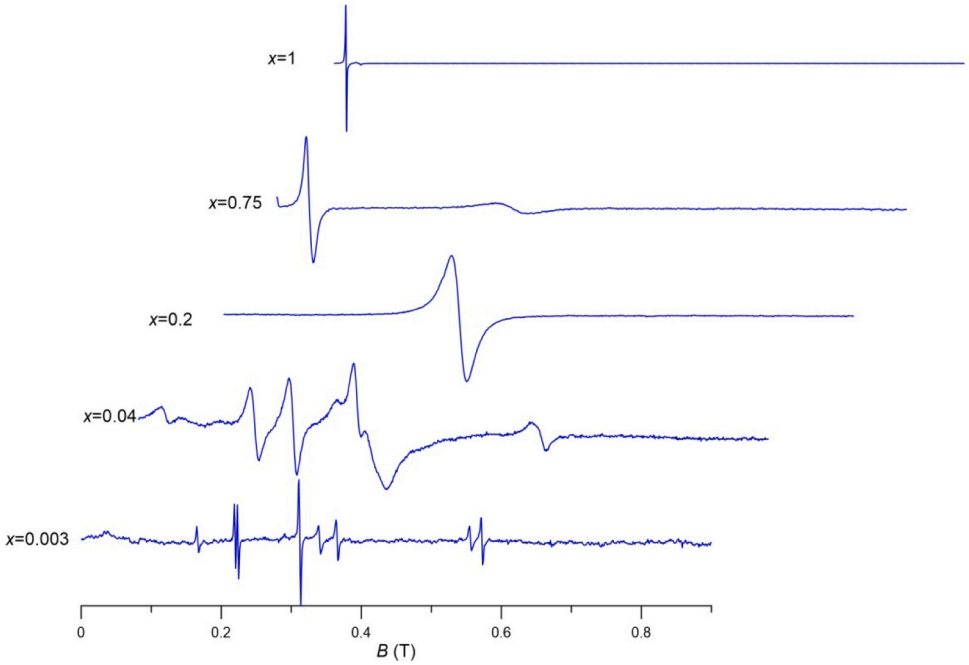

Fig. 3. Room-temperature X-band derivative-of-absorption EMR spectra of $Fe_xGa_{1-x}BO_3$ single crystals with different x shown alongside the curves.

be oriented by an external magnetic field, similarly to those of diluted paramagnetic ions. However, the magnetic susceptibility of a superparamagnetic system is usually much larger than that of a paramagnetic one. In contrast, if the relaxation is slow, $\tau \gg t_m$, one observes quasi-static properties, *viz.,* a blocked state similar to that of magnetically ordered crystals. The blocking temperature T_{bloc}, separating the two states is usually defined as the temperature at which $t_m = \tau$, so that it depends on the temporal window of the experimental technique [27]. Obviously, in a statistical ensemble of particles with different volumes, $E_{barrier}$ and T_{bloc} will be distributed.

Besides EMR, amongst most effective techniques for characterizing magnetic materials are (i) DC (direct current) and (ii) AC (alternating current) SQUID magnetometry [27]. In the case (i), the sample is magnetized in a constant field B_{dc} and the corresponding magnetization M_{dc} is measured. In the case (ii), an alternating magnetizing field of frequency f is applied, inducing a time-dependent magnetization with a phase lag. This behaviour is usually described by introducing in-phase, M' and out-of-phase, M'' magnetizations arising, respectively, from reversible and dissipative processes. Thus, the ac magnetometry gives information on the magnetization dynamics in magnetic phase transitions, relaxation, spin reorientation, *etc*. The measuring time in this case is usually taken as $t_m = 1/2\pi f$ [27].

In this paper, we report EMR and SQUID studies of mixed iron-gallium borate, $Fe_xGa_{1-x}BO_3$, crystals with different x.

2. Experimental samples

$Fe_xGa_{1-x}BO_3$ single crystals were synthesized using a standard solution in the melt technique [24]. Ga_2O_3, Fe_2O_3 and B_2O_3 were used as crystal-forming reagents and B_2O_3, PbO and PbF_2, as solvents. A typical composition of the reagents (in wt%) was as follows: $Fe_2O_3 + Ga_2O_3$ (5.73), B_2O_3 (51.23), PbO (29.31), and PbF_2 (13.73). The synthesized crystals had the shape of hexagonal plates with the dimensions of a few millimetres in the basal plane and about 50 μm in thickness. Inasmuch as the contents of iron and gallium in the crystals substantially differ from those in the charge [23], we have determined the former x using Energy Dispersive X-Ray Spectroscopy (EDS) and X-ray fluorescence (XRF) analysis; Scanning Electron Microscopy (SEM) has been used to map the crystals. The SEM and EDS studies were carried out with a JSM 6360 A SEM (JEOL) at 20 keV. The images and EDS data were collected using, respectively, a secondary electron detector and EX54175JMU EDS detector at a working distance of 10 mm. To prevent excessive charging, the samples were metallized by gold sputtering before the examination. The Fe:Ga ratio was then determined from the EDS spectra using the DTSA-II software (NIST) [31], after measuring reference spectra for $FeBO_3$ ($x = 1$) and $GaBO_3$ ($x = 0$). The XRF studies were carried out with an ElvaX spectrometer that allows identifying elements from Na to U.

Fig. 1 shows histograms of the distribution of x for crystals extracted from two crucibles with $x_{charge} = 0.10$ and 0.25. A significant distribution of iron content in these crystals is observed, with mean x-values of 0.21 and 0.32 and standard deviations of 0.023 and 0.079, respectively. For $x_{charge} = 0.10$, the mean x-value in the crystals is much higher than in the charge and the distribution of x is relatively narrow. For $x_{charge} = 0.25$, the mean x-value is close to that in the charge; meanwhile, the distribution of x is quite large.

Fig. 2 shows SEM images of $Fe_xGa_{1-x}BO_3$ single with $x = 0.200$ (the XFR data). Globally, the EDX abundance maps for Fe and Ga Kα lines evidence more or less random distributions of Fe and Ga in the volume of the crystal probed by the electron beam.

The iron contents in the crystals were also determined by XRF analysis. For x-values of 0.0354, 0.123, 0.155, 0.162, 0.289, 0.736, 0.81 and 0.845 determined by EDS, by XRFA we have found, respectively, 0.042, 0.199, 0.2016, 0.2091, 0.323, 0.666, 0.744 and 0.833. The discrepancy between the data of the two techniques can be due to the difference in depth penetration of the incident beam: between 2 and 3 μm for 20 keV electrons and *ca.* 900 μm, for X-rays of the same energy (Rh Kα line of most XRF spectrometers [32]). In what follows we are using the XRF data.

3. EMR studies

The EMR studies of $Fe_xGa_{1-x}BO_3$ single crystals were carried out with a commercial X-band (9.464 GHz) Bruker spectrometer in the temperature range T from 4 to 350 K and magnetizing fields up to 1 T applied in the basal plane of the crystals. A detailed account of the results on the electron paramagnetic resonance (EPR) and antiferromagnetic resonance (AFMR) studies of $Fe_xGa_{1-x}BO_3$ crystals respectively with $x = 0.003$ and $0.34 \leqslant x \leqslant 1.0$ has been published elsewhere [22,25]. In this

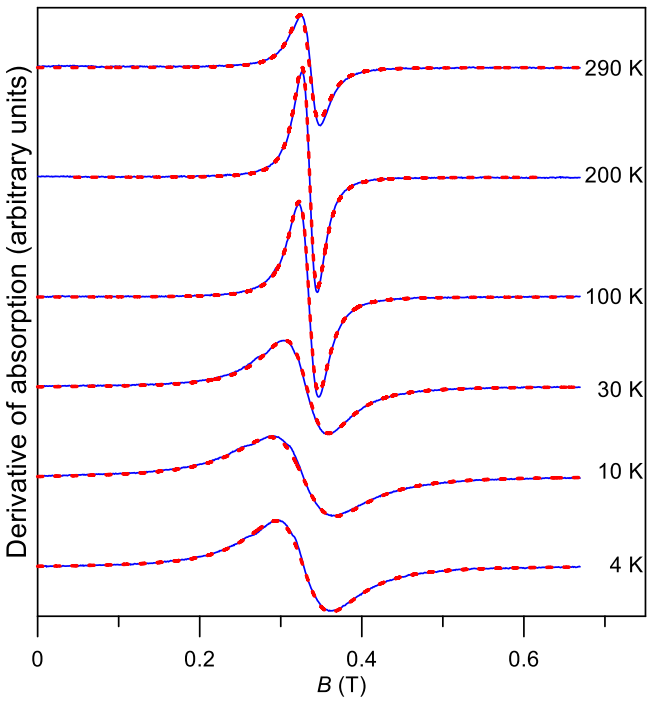

Fig. 4. Experimental (continuous, blue online) and simulated (dashed, red online) X-band EMR derivative of absorption spectra of $Fe_xGa_{1-x}BO_3$ single crystal with $x = 0.200$ crystal at different temperatures shown alongside the curves.

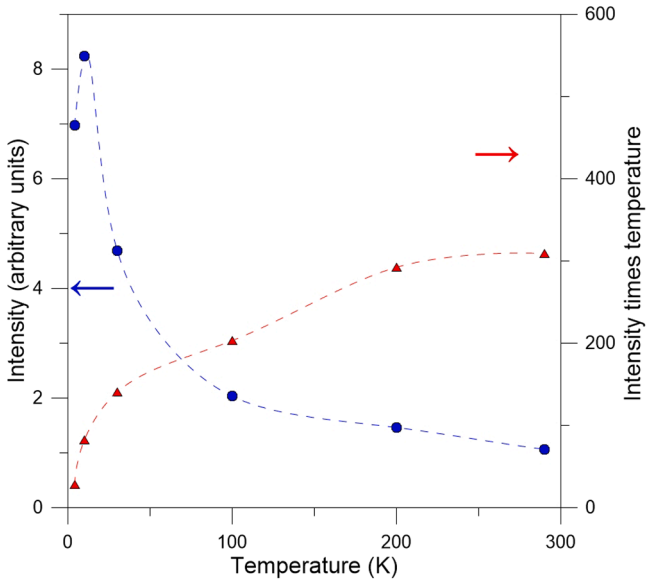

Fig. 5. Temperature dependence of the integral resonance line intensity (circles, blue online, left vertical axis) and of the integral intensity times temperature product (triangles, red online, right vertical axis) for $Fe_xGa_{1-x}BO_3$ single crystal with $x = 0.200$ crystal. The dashed lines are guides for the eyes.

paper we provide only a synopsis of these results.

Fig. 3 shows the evolution of the EMR spectra of $Fe_xGa_{1-x}BO_3$ single crystals with decreasing x in the range of $0.003 \leqslant x \leqslant 1.0$. For crystals with $x = 1.0$ and 0.75, a low-field resonance line is observed below the T_N, respectively, 348 and 300 K [22]. This line has been identified as a low frequency AFMR arising from magnetically ordered crystal regions [22]. For crystals with $x < 1$, a broad resonance line with an effective g-factor $g_{eff} = 2.0$ occurs at higher magnetic fields. At temperatures

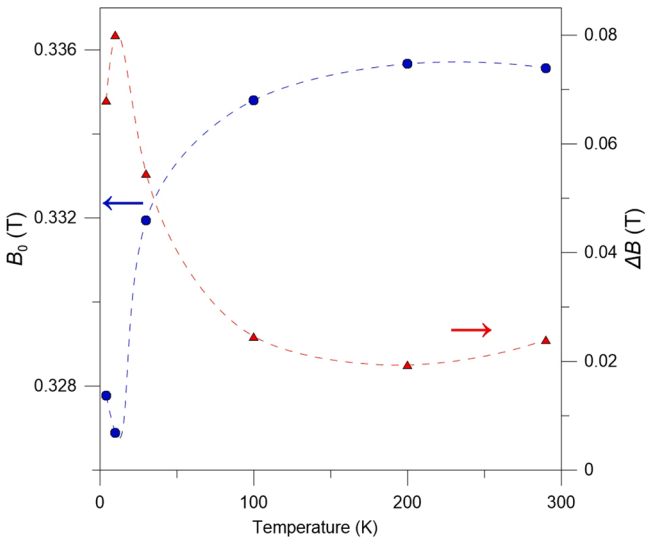

Fig. 6. Temperature dependence of the resonance field (circles, blue online, left vertical axis) and the peak-to-peak derivative-of-absorption linewidth (triangles, red online, right vertical axis) for $Fe_xGa_{1-x}BO_3$ single crystal with $x = 0.200$ crystal. The dashed lines are guides for the eyes.

below T_N, this line is ascribed to the cluster magnetic resonance (CMR), *i.e.*, the EMR arising from partially magnetically ordered regions, and in the vicinity of T_N it is due to a superposition of CMR and EPR. The crystals with $x = 0.003$ and 0.04 show only the EPR spectra of diluted iron ions; the spectrum for $x = 0.04$ is severely broadened by dipole-dipole interactions.

The EMR spectrum for $x = 0.200$ crystal consists of a single line with $g_{eff} \approx 2.0$, see Fig. 4. This line has been previously ascribed to CMR [22]. In contrast, the low-field AFMR line observed at higher x-values in this crystal is absent in the whole temperature range [22]; consequently, the antiferromagnetism does not occur in this case. Below, we focus on the CMR for this crystal. In order to extract the spectra parameters: the resonance field, B_0 and the peak-to-peak derivative-of-absorption linewidth, ΔB, the experimental spectra were fitted by Lorenzian lineshapes, as shown in Fig. 4.

Fig. 5 clearly shows that the intensity of this resonance does not follow the T^{-1} Curie law, corroborating its attribution to magnetic clusters. On the other hand, as far as the EMR line at $g_{eff} \approx 2.0$ is present in all crystals with higher x [22], we can conclude that in such crystals long-range and short-range (cluster-type) magnetic ordering coexist.

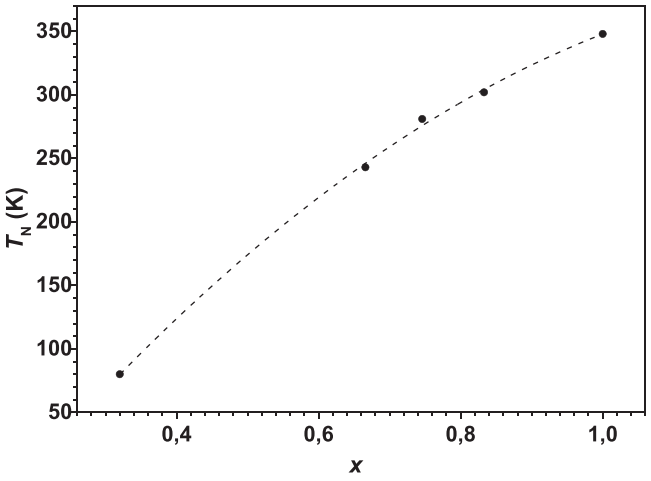

Fig. 7. The N é el temperature for $Fe_xGa_{1-x}BO_3$ single crystals with different x. The dashed line is a guide for the eyes.

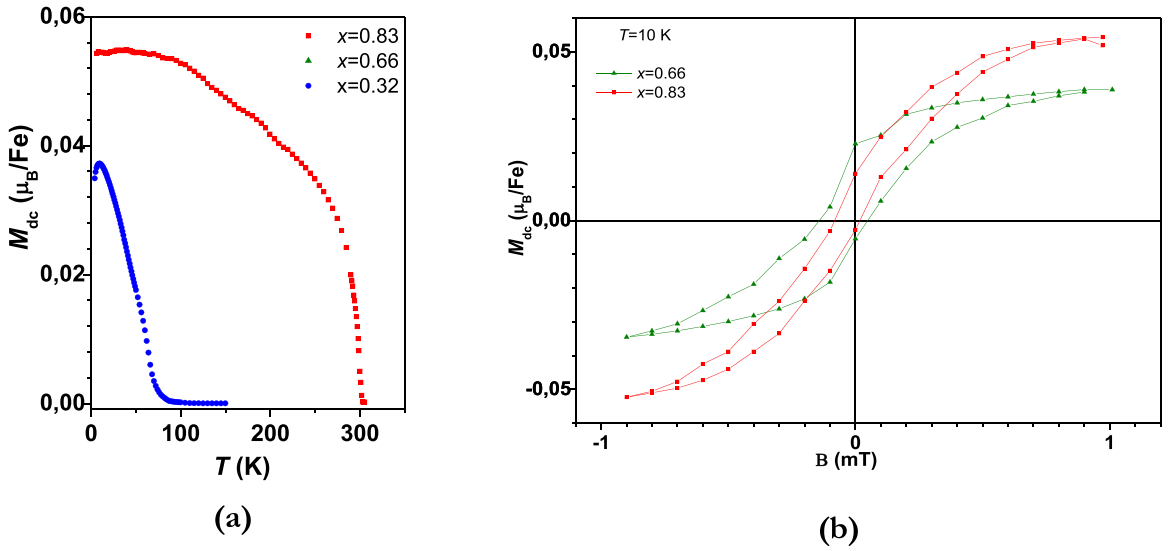

Fig. 8. Temperature dependence of the magnetization measured in a 0.972 mT DC magnetic field applied in the basal plane for $Fe_xGa_{1-x}BO_3$ single crystals with $x = 0.32$ and 0.83 (a); magnetization curves for $x = 0.66$ and 0.83 crystals at 10 K (b).

Fig. 6 shows B_0 and ΔB at different temperatures. As one can see, at lower temperatures the CMR line slightly shifts towards lower fields and considerably broadens. The decrease of B_0 at low temperatures is characteristic of superparamagnetic behaviour [33].

4. SQUID studies

The field and temperature dependences of the magnetic moments of various $Fe_xGa_{1-x}BO_3$ single crystals were measured with a Quantum Design SQUID MPMS-7XL magnetometer. The DC and AC magnetization measurements were performed with either the standard linear transport or the more sensitive Reciprocating Sample Option transport. For AC measurements, special care was taken to work in zero-field conditions. All samples were accurately weighed using a Mettler-Toledo MX5 microbalance. The magnetometry studies of $Fe_xGa_{1-x}BO_3$ single crystals with $0.04 \leq x \leq 0.83$ were carried out in the temperature range from 2 to 320 K. Further experimental details (sample mounting, magnetic field preparation, data treatment) are given in Electronic Supplementary Material (ESI-file) for each crystal (Figs. S4 to S47).

Fig. 7 shows T_N for crystals with different x. The dependence of T_N on x is in good accordance with that previously determined by EMR [22]. Note that SQUID magnetometry allows more accurate determination of T_N in comparison with EMR. With diamagnetic dilution, T_N decreases because of a decrease of the effective exchange field, since the concentration of paramagnetic ions and the average number of their paramagnetic neighbours decrease.

Fig. 8a shows the temperature dependences of the magnetization M_{dc} of $Fe_xGa_{1-x}BO_3$ single crystals with $0.32 \leq x \leq 0.83$ in a 0.972 mT magnetic field applied in the basal plane of the sample. For these x-values the magnetization is due to magnetic ordering, as confirmed by our EMR studies [22]: indeed, in this case below T_N the AFMR line is observed, *cf.* Fig. 3 above. The decrease of M_{dc} with diamagnetic dilution, see Fig. 8, is due to the decrease in the contents of the paramagnetic ions in the crystals. Besides, one can see that with decreasing x the increase of M_{dc} about the N é el temperature becomes smoother. This behaviour can be explained by a spatial distribution in T_N, as occurs in mixed crystals [34].

In cooling from T_N, M_{dc} first increases, then passes through a maximum and finally decreases, see Fig. 8a. Earlier we published M_{dc} *vs* T for $x = 0.32$ crystal measured in a 10 mT DC magnetic field that shows similar behaviour [22]. This behaviour is indicative of another magnetic transition occurring well below the N é el temperature. This transition is

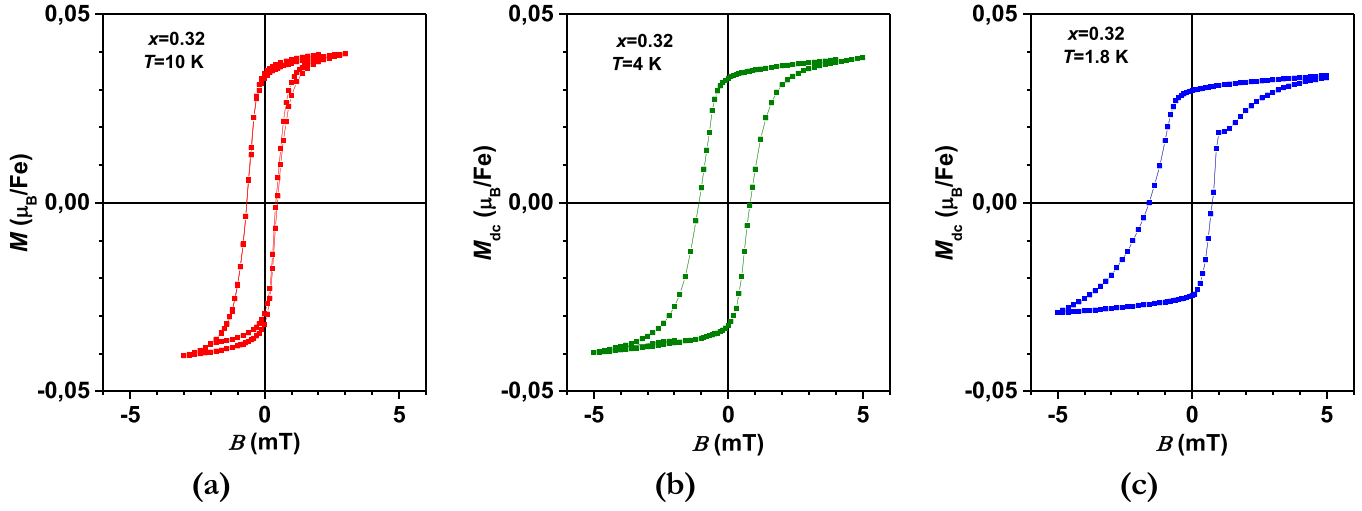

Fig. 9. Magnetization curves for $Fe_xGa_{1-x}BO_3$ single crystal with $x = 0.32$ at 10 (a), 4 (b) and 1.8 (c) K.

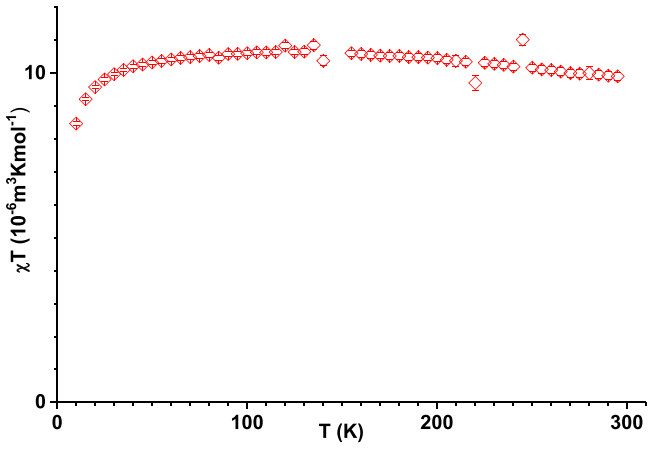

Fig. 10. Temperature dependence of χT for $Fe_xGa_{1-x}BO_3$ single crystal with $x = 0.200$ in a magnetic field of 1 T.

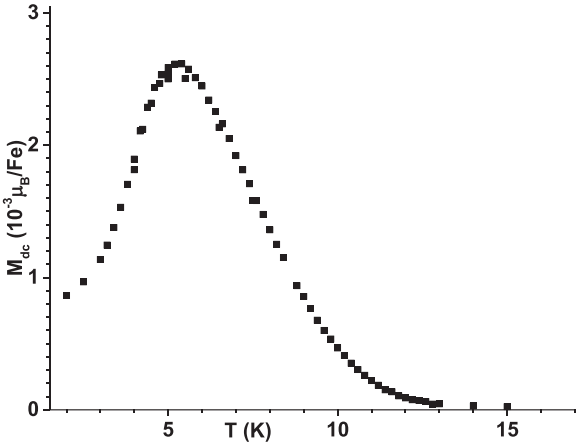

Fig. 11. Temperature dependence of zero-field M_{dc} for $Fe_xGa_{1-x}BO_3$ single crystal with $x \approx 0.21$.

most pronounced for crystal with $x = 0.32$, meanwhile it is systematically present in crystals with $0.34 \leq x \leq 0.85$. Indeed, our previous AFMR studies of the temperature dependence of the resonance field in crystals with $0.34 \leq x \leq 0.85$ [22] have shown an unusual shift of the

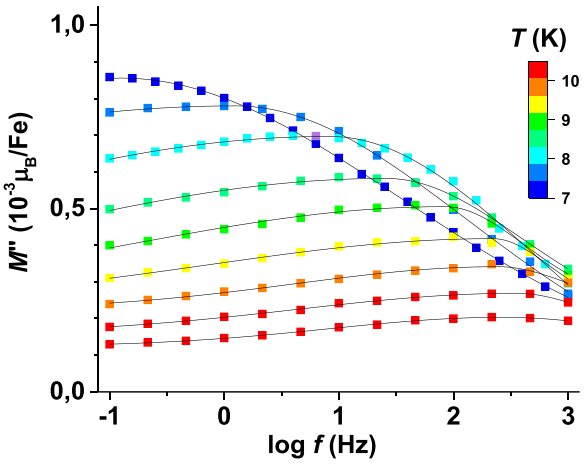

Fig. 13. Frequency dependence of M'' on $\log f$ measured in a 0.38 mT AC magnetic field for $Fe_xGa_{1-x}BO_3$ single crystal with $x \approx 0.21$ at temperatures between 6.5 and 10 K (squares). The curves are asymmetric Gaussian fits, see details below and in ESI.

AFMR line to higher field at low temperatures. This behaviour is in contrast to those for crystals with $x = 1$ and it had been described in terms of decreasing the Dzyaloshinskii–Moriya field and the resulting magnetization in the basal plane of the crystals. The present SQUID measurements confirm this finding. The magnetic field dependences of the magnetization for $x = 0.66$ and 0.83 single crystals are shown in Fig. 8b.

For $x = 0.32$ crystal, the magnetization curves at temperatures below the abovementioned transition, see Fig. 9, show that the saturation and remanent magnetizations decrease with decreasing temperature, whereas the coercive field shows an opposite tendency. We ascribe this behaviour to a Morin-type transition [22,35] with a characteristic temperature $T_M = 10K$ for this crystal. In the present case, one can assume that below T_M the weak ferromagnetism vanishes and the crystal transforms from an *easy-plane* to an *easy-axis* antiferromagnet, the sublattice magnetizations lying along the trigonal axis. Such a transition has been earlier observed in α-Fe_2O_3 (hematite) both undiluted and diluted with diamagnetic ions [36]. Indeed, a very similar behaviour is observed in Figs. 4 and 5 in the paper by P. J. Besser *et al.* [36], notwithstanding the fact that in mixed crystals the transition is smoothed because of randomness in the spatial distribution of paramagnetic ions.

Further DC measurements of the temperature dependence of the χT

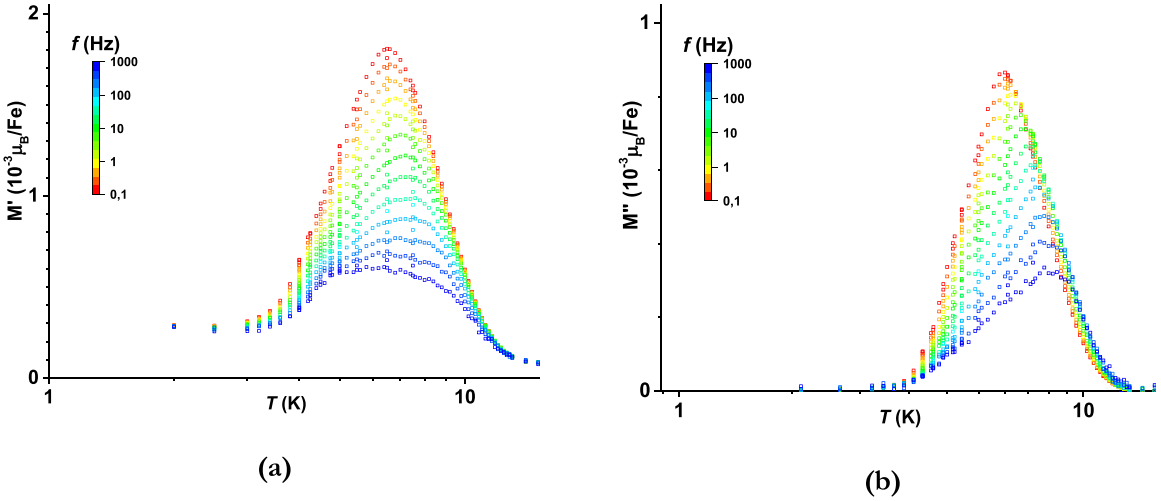

Fig. 12. M' (a) and M'' (b) for $Fe_xGa_{1-x}BO_3$ single crystal with $x \approx 0.21$, measured between 6 and 15 K in a 0.38 mT AC magnetic field for 13 frequencies between 0.1 and 997 Hz. A logarithmic scale for T has been used.

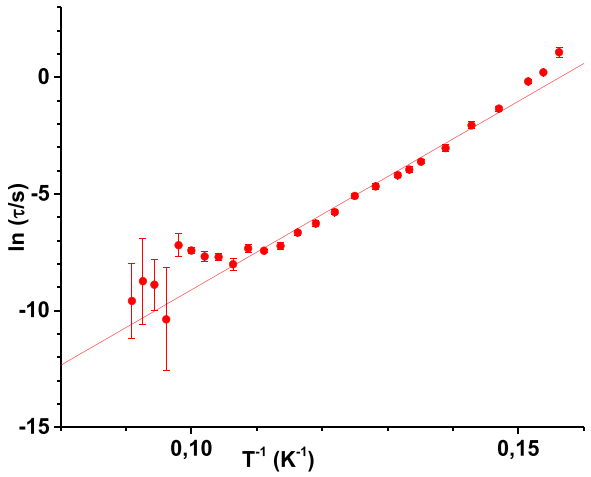

Fig. 14. Arrhenius plot for the $Fe_xGa_{1-x}BO_3$ single crystal with $x \approx 0.21$ (red circles), with corresponding linear fit.

product, χ being the molar magnetic susceptibility, carried out in a magnetic field of 1 T were performed on a crystal with $x = 0.200$, see Fig. 10. The plateau *ca* 10×10^{-6} m^3 $K\ mol^{-1}$, observed at higher temperatures, is significantly lower than the expected χT value of 55.0×10^{-6} m^3 $K\ mol^{-1}$ for diluted high-spin Fe(III) with $S = 5/2$ and a *g*-factor of 2.0. Moreover, below 40 K χ does not follow the T^{-1} Curie law.

The variable temperature measurements of M_{dc} for the crystal with $x \approx 0.21$ carried out without specially applying a magnetizing field show the occurrence of magnetization below 13 K, *cf.* Fig. 11. In cooling the crystal, M_{dc} first increases, next decreases.

To get a closer insight in the dynamic behaviour of magnetization in this *x*-range, M_{ac} for $x \approx 0.21$ crystal was measured for several frequencies *f* of the magnetizing field. As can be seen in Fig. 12, at certain temperatures both M' and M'' show maxima and the positions of these maxima are frequency-dependent. Obviously, here we are dealing with an energy barrier for the magnetic relaxation, as expected for superparamagnetic particles with frequency-dependent T_{bloc}.

As we have seen in the Introduction, $\tau = 1/2\pi f_{max}$, where f_{max} is the position of the maximum of frequency dependence of M'' at fixed temperature, see Fig. 13. The maximum was determined by fitting asymmetric Gaussian shapes to the corresponding dependences. This asymmetry can be related to the size distribution of the superparamagnetic clusters.

Fig. 14 shows the Arrhenius plot of $\ln \tau$ *vs.* $1/T$. A linear fit to Eq. (1) over the 6.8–9.4 K range yields $\tau_0 = 9.8(51) \times 10^{-12}$ s and $E_{barrier} = 13.9$ (3) meV. These values are characteristic of spin glasses, magnetic clusters and molecular complexes showing a slow relaxation of the magnetization, so it supports the hypothesis of small magnetic clusters in the crystal matrix. Using the value of $E_{barrier} = KV$, the frequency dependence of M'' can be satisfactorily simulated with the mean cluster diameter of 7.2 Å, as described in ESI (see Fig. S47). This value gives a reasonable idea of the magnetic cluster sizes in $x \approx 0.2$ crystal, as will be shown in the following subsection.

We can assume that the nature of the magnetization observed in $0.32 \leq x \leq 0.85$ crystals on the one hand and $x \approx 0.2$ on the other hand, *cf.* Figs. 8a and 11 is different. Indeed, in the first case, the magnetization is due to weak ferromagnetism, as confirmed by our EMR studies [22]. We can see that the unexpected shift of the AFMR line to higher field [22] occurs at the same temperature as the decrease of the DC magnetisation, see Fig. 8a. Therefore, this decrease is related to the magnetic transition occurring in magnetically ordered parts of the crystals. In contrast, our EMR studies, see Fig. 4, show the absence of long-range ordering in the crystal with $x \approx 0.2$. In this case, the magnetization decrease at the lowest temperature, see Fig. 11, is caused by a superparamagnetic behaviour, *viz.*, blocking the reorientations of the magnetic moments of iron clusters below T_{bloc}. Moreover, the temperature dependence of the AC magnetization for $x = 0.32$ crystal show that the position of the magnetization maximum is frequency-independent, see Fig. S29 in ESI. In contrast, for $x \approx 0.21$ crystal the frequency-dependent magnetization maxima are observed, see Fig. 12, as expected for superparamagnetic clusters.

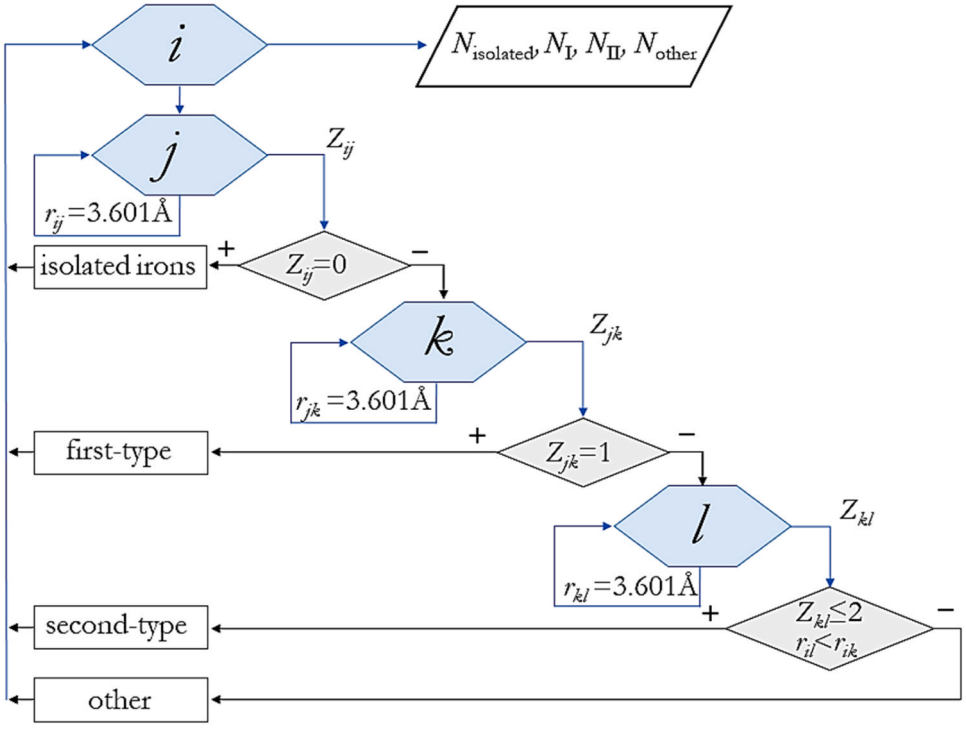

Fig. 15. Block diagram of the simulation code used to visualize iron clusters in Fe_xG_{a1}-xBO_3 crystals.

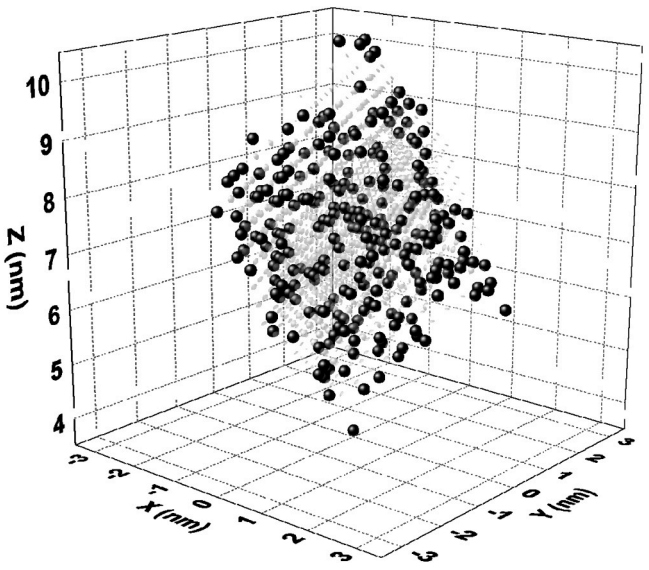

Fig. 16. Spatial distribution of Fe (black spheres) and Ga (light grey spheres) ions in $Fe_xGa_{1-x}BO_3$ crystal for x= 0.2.

5. Computer modelling of the magnetic cluster phase in mixed iron-gallium borates

In $FeBO_3$ the nearest environment of an iron ion consists of $Z = 6$ Fe^{3+} ions located at a distance of 3.601 Å in the planes above and below this ion [1]. In diamagnetically diluted $Fe_xGa_{1-x}BO_3$ crystals ($x < 1$), a part of iron ions are randomly substituted by gallium ions; therefore, for different irons Z can vary between 0 and 6. In order to visualize the spatial distribution of dia- and paramagnetic ions and estimate the size of iron clusters in mixed $Fe_xGa_{1-x}BO_3$ crystals, we have put forward a Monte Carlo computer simulation code, see Fig. 15.

In the first step, we calculate the number of the nearest iron neighbours Z_{ij} for each ith iron ion. If $Z_{ij} = 0$, we are dealing with isolated irons ions. In the second step, we calculate the number of nearest iron ions, Z_{jk} for each jth iron. If $Z_{jk} = 1$ for all j, we are dealing with a first-type cluster. In the third step, we determine the number Z_{kl} of the nearest iron neighbours of each kth ion. If $Z_{kl} \leq 2$ and the distance r_{li} between l and i ions is less than distance r_{ki} between k and i ions, the object is considered as a cluster of a second type.

Below we demonstrate the simulation results for a crystal with $x = 0.2$, in which case the probabilities of iron or gallium occupying a given site are 0.2 or 0.8, respectively. Fig. 16 shows a computer simulated spatial distribution of iron and gallium ions in this crystal. One can clearly see nanoscopic iron clusters occurring at this x-value. Such clusters are expected to be single-domain and show a superparamagnetic behaviour [27,33].

Fig. 17 shows examples of the first- and second type clusters (see ESI for more examples).

In this fashion, we have identified the clusters spanning up to four Fe-Fe distances. Fig. 18 shows the percentage of iron ions in different size clusters.

Further details of computer simulations of iron clustering in iron-gallium borates can be found in ESI in Figs. S48 and S49.

6. Summary and conclusions

Iron-gallium borates, $Fe_xGa_{1-x}BO_3$ possess an extremely wide range of magnetic properties depending on their diamagnetic dilution factor, $1 - x$. Our EMR and SQUID studies of these crystals have shown that for $x \gtrapprox 0.32$ these crystals are antiferromagnetic with weak ferromagnetism. The N é el temperature is lowered with decreasing x. For crystals at intermediate dilution, $0.2 < x < 0.32$, both EMR and SQUID data, in particular, the temperature dependences of the resonance intensity and linewidth on the one hand and a pronounced frequency dependence of the imaginary part of the magnetization on the other hand attest the presence of magnetic cluster phase showing a superparamagnetic behaviour.

Interestingly, in $x \approx 0.32$ crystals one more transition has been found well below the N é el temperature. It manifests itself in a decrease of spontaneous magnetization in the basal plane of the crystals; therefore, we tentatively identify it as a Morin-type transition. Inasmuch as the magnetization in these crystals is due to weak ferromagnetism, this decrease is related to the magnetic transition occurring in magnetically ordered parts of the crystals. On the other hand, in the crystals with $x \approx 0.2$ the decrease of magnetization at low temperatures is caused by blocking the reorientations of the magnetic moments of the superparamagnetic iron clusters.

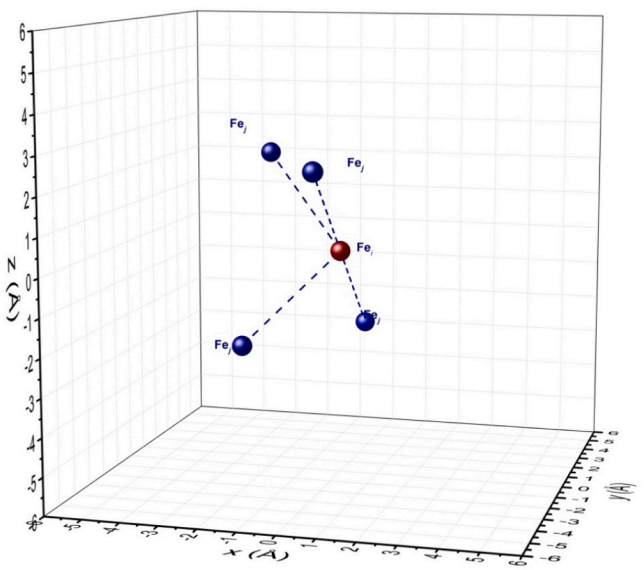

(a)

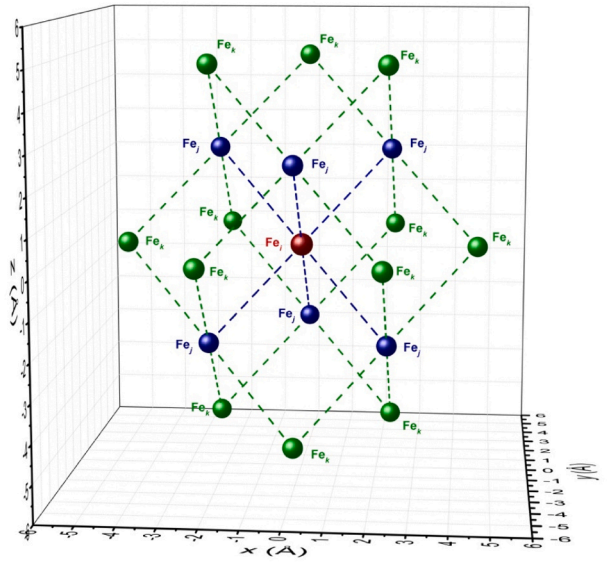

(b)

Fig. 17. Examples of clusters of the first (a) and second (b) types in $Fe_xGa_{1-x}BO_3$ crystal with x= 0.2.

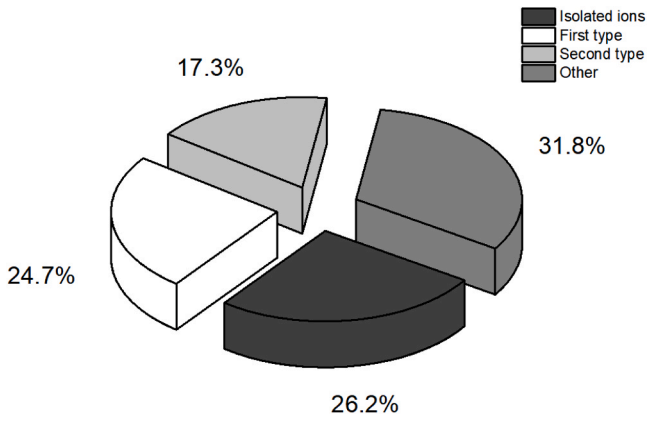

Fig. 18. Pie chart of the distribution of iron ions over different types of clusters in $Fe_xGa_{1-x}BO_3$ crystal with x= 0.2.

A computer simulation of the distribution of iron ions over clusters of different sizes for $x \approx 0.2$ crystal shows the predominance of small clusters having a size between one and four metal-to-metal (Fe–Fe) distances. This finding is consistent with the superparamagnetic behaviour witnessed in this study.

CRediT authorship contribution statement

Kira Seleznyova: Conceptualization, Methodology, Software, Formal analysis, Investigation, Writing – original draft, Writing – review & editing, Visualization, Supervision. **Mark Strugatsky:** Conceptualization, Methodology, Formal analysis, Investigation, Writing – original draft, Writing – review & editing, Supervision, Funding acquisition. **Sergey Yagupov:** Conceptualization, Methodology, Validation, Investigation, Resources. **Yuliya Mogilenec:** Conceptualization, Methodology, Software, Formal analysis, Investigation, Visualization. **Patrick Rosa:** Conceptualization, Software, Validation, Formal analysis, Investigation, Resources, Data curation, Writing – original draft, Visualization. **Mathieu Gonidec:** Conceptualization, Validation, Formal analysis, Investigation, Resources, Data curation, Writing – original draft, Visualization. **Janis Kliava:** Conceptualization, Methodology, Software, Formal analysis, Investigation, Writing – original draft, Writing – review & editing, Supervision.

Declaration of Competing Interest

The authors declare that they have no known competing financial interests or personal relationships that could have appeared to influence the work reported in this paper.

Data availability

No data was used for the research described in the article.

Acknowledgement

This work is funded by the RSF and the Ministry of Education, Science and Youth of the Republic of Crimea, project number 22-22-20112, in terms of computer modeling of the magnetic cluster phase in mixed iron-gallium borates.

Appendix A. Supporting information

Supplementary data associated with this article can be found in the online version at doi:10.1016/j.jallcom.2023.173105.

References

[1] R. Diehl, W. Jantz, B.I. Nolang, W. Wettling, in: E. Kaldis (Ed.), Current Topics in Materials Science, 11, Elsevier, New-York, 1984, pp. 241–387.
[2] D. Afanasiev, I. Razdolski, K.M. Skibinsky, D. Bolotin, S.V. Yagupov, M. B. Strugatsky, A. Kirilyuk, Th. Rasing, A.V. Kimel, Laser excitation of lattice-driven anharmonic magnetization dynamics in dielectric FeBO3, Phys. Rev. Lett. 112 (2014), 147403.
[3] M. Eibshutz, M.E. Lines, Sublattice magnetization of FeBO3 single crystals by mössbauer effect, Phys. Rev. B 7 (1973) 4907–4915.
[4] A.M. Kalashnikova, A.V. Kimel, R.V. Pisarev, V.N. Gridnev, P.A. Usachev, A. Kirilyuk, Th Rasing, Impulsive excitation of coherent magnons and phonons by subpicosecond laser pulses in the weak ferromagnetFeBO3, Phys. Rev. B 78 (2008), 104301.
[5] Yu.N. Mitsay, K.M. Skibinsky, M.B. Strugatsky, A.P. Korolyuk, V.V. Tarakanov, V. I. Khizhnyi, J. Magn. Magn. Mater. 219 (2000) 340–348.
[6] K. Parlinski, J. Łażewski, P.T. Jochym, A. Chumakov, R. Rüffer, G. Kresse, Influence of magnetic interaction on lattice dynamics of FeBO3, Europhys. Lett. 56 (2001) 275–281.
[7] M. Strugatsky, K. Seleznyova, V. Zubov, J. Kliava, New insight in the nature of surface magnetic anisotropy in iron borate, Surf. Sci. 668 (2018) 80–84.
[8] M. Strugatsky, K. Seleznyova, S. Yagupov, A. Drovosekov, J. Kliava, Nature of magnetocrystalline anisotropy in the basal plane of iron borate, J. Magn. Magn. Mater. 442 (2017) 417–422.
[9] E.M. Maksimova, I.A. Nauhatsky, M.B. Strugatsky, V.E. Zubov, Surface magnetism of real iron borate monocrystals, J. Magn. Magn. Mater. 322 (2010) 477–480.
[10] L.V. Velikov, A.S. Prokhorov, E.G. Rudawevskii, V.N. Seleznev, JETP 66 (1974) 1847.
[11] M.B. Strugatsky, K.M. Skibinsky, V.V. Tarakanov, V.I. Khizhnyi, Fine structure of Gakel'–Turov oscillations in iron borate, J. Magn. Magn. Mater. 241 (2002) 330–334.
[12] M.B. Strugatsky, K.M. Skibinsky, Acoustic resonances in antiferromagnet FeBO3, J. Magn. Magn. Mater. 309 (2007) 64–70.
[13] I.A. Troyan, M.I. Eremets, A.G. Gavrilyuk, I.S. Lyubutin, V.A. Sarkisyan, JETP Lett. 78 (2003) 13.
[14] A.M. Kalashnikova, A.V. Kimel, R.V. Pisarev, V.N. Gridnev, P.A. Usachev, A. Kirilyuk, Th. Rasing, Impulsive generation of coherent magnons by linearly polarized light in the easy-plane antiferromagnet FeBO3, Phys. Rev. Lett. 99 (2007), 167205.
[15] K. Seleznyova, N. Sergeev, M. Olszewski, P. Stepien, S. Yagupov, M. Strugatsky, J. Kliava, (11)B MAS NMR study of Ga1-xFexBO3 mixed crystals, Solid State Nucl. Magn. Reson. 70 (2015) 38–42.
[16] A.V. Malakhovskii, I.S. Edelman, Phys. Status Solidi (b) 74, K145 (1976).
[17] W. Jantz, J.R. Sandercock, W. Wettling, J. Phys. C 9 (1976) 2229.
[18] V.N. Seleznev, Thesis, Simferopol State University, 1988.
[19] V. Potapkin, A.I. Chumakov, G.V. Smirnov, J.-Ph Celse, R. Rüffer, C. McCammon, L. Dubrovinsky, The 57Fe synchrotron mössbauer source at the ESRF, J. Synchrotron Radiat. 19 (2012) 559–569.
[20] V. Potapkin, A.I. Chumakov, G.V. Smirnov, R. Rüffer, C. McCammon, L. Dubrovinsky, Angular, spectral, and temporal properties of nuclear radiation from a57Fe synchrotron Mössbauer source, Phys. Rev. A 86 (2012), 053808.
[21] S. Yagupov, M. Strugatsky, K. Seleznyova, Yu Mogilenec, N. Snegirev, N. Marchenkov, A. Kulikov, Ya Eliovich, K. Frolov, Yu Ogarkova, I. Lyubutin, Development of a synthesis technique and characterization of high-quality iron borate FeBO3 single crystals for applications in synchrotron technologies of a new generation, Cryst. Growth Des. 18 (2018) 7435–7440.
[22] K. Seleznyova, M. Strugatsky, S. Yagupov, Yu Mogilenec, A. Drovosekov, N. Kreines, P. Rosa, J. Kliava, Electron magnetic resonance of iron-gallium borate single crystals, J. Appl. Phys. 125 (2019), 223905.
[23] S. Yagupov, E. Maksimova, I. Nayhatsky, V. Yagupov, E. Milyukova, K. Seleznyova, M. Strugatsky, in: Proceedings of the Int. Conf. on Oxide Materials for Electronic Engineering OMEE-2014, 207.
[24] S. Yagupov, M. Strugatsky, K. Seleznyova, E. Maksimova, I. Nauhatsky, V. Yagupov, E. Milyukova, J. Kliava, Fe x Ga1−x BO3 single crystals: synthesis and characterization, Appl. Phys. A 121 (2015) 179–185.
[25] K. Seleznyova, M. Strugatsky, S. Yagupov, N. Postivey, A. Artemenko, J. Kliava, Electron paramagnetic resonance of Fe3+in gallium borate: superposition model analysis: EPR of Fe3+in gallium borate: superposition model analysis, Phys. Stat. Sol. B 251 (2014) 1393–1400.
[26] R.D. Shannon, Revised effective ionic radii and systematic studies of interatomic distances in halides and chalcogenides, Acta Cryst. A 32 (1976) 751–767.
[27] J.L. Dormann , D. Fiorani , E. Tronc , in: Advances in Chemical Physics, I. Prigogine , Stuart A. Rice eds., John Wiley & Sons, 98 (1997) 283–494.
[28] D. Reta, N.F. Chilton, Uncertainty estimates for magnetic relaxation times and magnetic relaxation parameters, Phys. Chem. Chem. Phys. 21 (2019) 23567–23575.
[29] D. Gatteschi, R. Sessoli, J. Villain, Molecular Nanomagnets, Oxford University Press, 2006.
[30] S. Chikazumi, Phys. Ferromagn. (1997).
[31] D.E. Newbury, N.W.M. Ritchie, Performing elemental microanalysis with high accuracy and high precision by scanning electron microscopy/silicon drift detector energy-dispersive X-ray spectrometry (SEM/SDD-EDS), J. Mater. Sci. 50 (2015) 493–518.
[32] https://physics.nist.gov/PhysRefData/FFast/html/form.html
[33] J. Kliava, in: Magnetic Nanoparticles Gubin, S.P. (Ed.), Wiley-VCH Verlag GmbH & Co. KGaA, Ch. 7 (2009) 255–302.

[34] H. Ikeda, M. Suzuki, M.T. Hutchings, J. Phys. Soc. Jpn 46 (1979) 1153.
[35] F.J. Morin, Phys. Rev. 78 (1950) 819.
[36] P.J. Besser, A.H. Morrish, C.W. Searle, Magnetocrystalline anisotropy of pure and doped hematite, Phys. Rev. 153 (1967) 632–640.